New Zealand Journal of Geology and Geophysics

ISSN: 0028-8306 (Print) 1175-8791 (Online) Journal homepage: www.tandfonline.com/journals/tnzg20

Fluid migration and permeability in evolving fault damage zones: a study of carbonate reservoir from Qingzhou, eastern China

Nianfa Yang, Rulang Wang, Xiaofeng Chen & Zonghu Liao

To cite this article: Nianfa Yang, Rulang Wang, Xiaofeng Chen & Zonghu Liao (2025) Fluid migration and permeability in evolving fault damage zones: a study of carbonate reservoir from Qingzhou, eastern China, New Zealand Journal of Geology and Geophysics, 68:5, 971-982, DOI: 10.1080/00288306.2025.2519724

To link to this article: https://doi.org/10.1080/00288306.2025.2519724

Published online: 26 Jun 2025.

NEW ZEALAND JOURNAL OF GEOLOGY AND GEOPHYSICS
2025, VOL. 68, NO. 5, 971–982
https://doi.org/10.1080/00288306.2025.2519724

Taylor & Francis
Taylor & Francis Group

RESEARCH ARTICLE

Fluid migration and permeability in evolving fault damage zones: a study of carbonate reservoir from Qingzhou, eastern China

Nianfa Yang [a,b], Rulang Wang[a], Xiaofeng Chen[c] and Zonghu Liao[a,b]

[a]State Key Laboratory of Petroleum Resources and Prospecting, College of Geosciences, China University of Petroleum, Beijing, People's Republic of China; [b]China-Portugal Joint Research Institute of Climate and Energy, China University of Petroleum, Beijing, People's Republic of China; [c]Boone Pickens School of Geology, Oklahoma State University, Stillwater, Oklahoma City, USA

ABSTRACT

Faults and fractures record history crustal deformation. The fault structure evolves as fault slip accumulates, and the fault damage zone structure is critical in controlling fluid migration and earthquakes. In this work, we investigated the internal structure and permeability characteristics of fault damage zones developed in the Cambrian-Ordovician carbonate strata in the Qingzhou area, eastern China using field investigation, outcrop rock sample analysis, and permeability tests. The results show: (1) The carbonate fault in Tuoshan Nan quarry is a large strike-slip fault with a 1-m-thick fault core; (2) Evidence of calcite cementation in the fault surfaces suggests that the carbonate fault damage zones are major fluid migration channels; (3) The calcite cementation together with fault gouge, in turn, form ultra-low permeability barriers at later stages of fault development. We anticipate that the fault evolved from a single slip surface to composite structures, determining the permeability structure crossing the fault damage zones, which provide insights for assessing the faulting activities in this region.

ARTICLE HISTORY
Received 3 August 2024
Accepted 9 June 2025

HANDLING EDITOR
Li-Wei Kuo

KEYWORDS
Carbonate rocks; fault core; damage zone; permeability; fluid flow; earthquake

Introduction

Fault damage zones can significantly impact fluid flow patterns in the subsurface and subsequently affect the pore pressure distribution (Nur and Booker 1972), which is critical to understanding the dynamism of earthquakes. A fault zone typically comprises a complex network of interconnected fault surfaces that separate pockets of fractured and crushed rocks (Davis et al. 1996). A mature fault zone typically comprises two components: the damage zone, composed of rock volumes that have undergone fracturing related to the fault, and a fault core, composed of cataclastic rocks with low permeability (Chester et al. 1993; Caine et al. 1996; Liao et al. 2017). Bedding surfaces and pre-existing structural fabrics are commonly preserved within the damage zones. The permeability characteristics of fault cores and damage zones differ due to the distinct deformation features they exhibit (Evans 1990; Antonellini and Aydin 1994, 1995; Evans et al. 1997; Knipe 1997; Manzocchi et al. 1999; Yielding et al. 1999; Wibberley and Shimamoto 2003).

In the oil field, it is generally accepted that the faults can juxtapose one reservoir section with another, creating the potential for cross-flow of petroleum between fault blocks. However, deformation and cementation within a fault can create a zone of ultra-low permeability, resulting in the fault damage zone acting as a barrier for oil flow. Whether the fault is a conduit (Caine et al. 1996; Shepherd 2009; Bense et al. 2013) or a barrier (Gale et al. 2007; He et al. 2021) for oil flow depends on many factors, including the structure of the fault and rock types, particularly for carbonate rocks (Olson 2003; Shipton et al. 2004; Bense and Person 2006). In this study, we investigated three faults developed within the Lower Palaeozoic carbonate unit in the Qingzhou area, eastern China. We studied the internal structure of these carbonate fault damage zones and their permeability characteristics.

Geological Settings

The study area is in the Qingzhou area on the west side of the Tancheng-Lujiang Fault Zone in eastern China (Figure 1), where active seismic events significantly impact the structural development. In the Qingzhou area, two main groups of faults constitute the 'X' shape with one striking NW-NNW (Qingzhou fault) and the other one in NE-NNE (Wujing fault) (Wang 1995). Due to the change of regional tectonic stress field, the two groups of faults experienced multi-stage activities. During the Late Triassic, the Tancheng-Lujiang Fault Zone exerted a downward and leftward traction on the western blocks, including the Qingzhou region. Under the combined influence of various factors such as boundary conditions, weak

CONTACT Zonghu Liao zong@cup.edu.cn

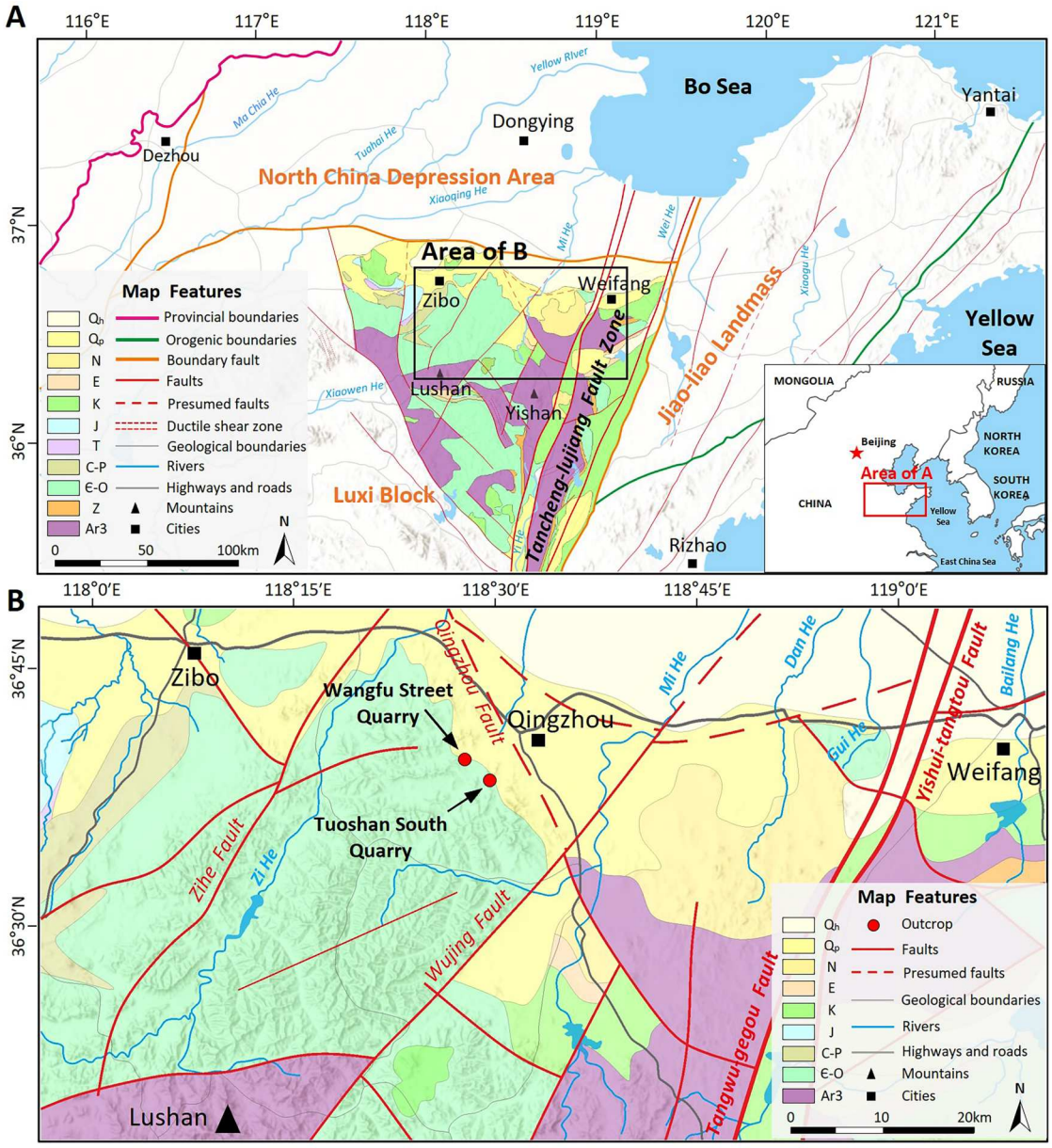

Figure 1. Geological map of the study area: (1) The lower right corner of the illustration delineates the eastern part of China with the red box highlighting the specific area designated as A; (2) The overall region is stratified into five distinct blocks by boundary faults and orogenic boundaries, with the central three blocks identified as the North China Depression, Jiao-liao Landmass, and Luxi Block. The study area is situated within the Luxi Block; (3) The symbology on the map features 'Qh' for Holocene, 'Qp' for Pleistocene, 'N' for Neogene, 'E' for Palaeogene, 'K' for Cretaceous, 'J' for Jurassic, 'T' for Triassic, 'C-P' for Carboniferous-Permian, 'Є-O' for Cambrian and Ordovician, 'Z' for Sinian, and 'Ar3' for Neoarchaean.

zones within the blocks manifested as NE-stepped secondary faults (Liu 1999). During the late Jurassic to the early Cretaceous, the Kula plate moved from the north to the west, resulting in an NWW-SE or NW-SE horizontal compression on the NE-trending eastern continental margin (Wang 1995; Yu 1992). As a result, the Luxi block further disintegrated to form a conjugated fault system, and a series of fault blocks bulged and fault-controlled basins were formed. In this stage, the NE-trending faults are dominated by right-lateral motion.

The Qingzhou area is located in the Luxi stratigraphic division (Shandong Provincial Bureau of Geology & Mineral Resources 1991; Wang 2011), and the outcropped strata are mainly Cambrian and Ordovician strata of carbonates. The strata is widely distributed, and we selected two major formations in this study: (1) The Bei'anzhuang section of the Majiagou Formation composed of grey to dark grey thick microcrystalline limestone and dolomitic limestone with dolomite in the upper and lower parts; (2) The upper part of the Sanshanzi Formation composed of grey medium-thick chert bands and nodular dolomite, with purple grey medium-thin fine-grained dolomite and bamboo-like dolomite in the middle part, and the medium-thick to thick microcrystalline dolomite with medium-thin fine-grained dolomite in the lower part.

Methods

We investigated two outcrops in the Qingzhou area, the Tuoshan Nan quarry and the Wangfu Street quarry (Figure 1(B)). Three geological sections were observed in Tuoshan Nan Quarry and one geological section was observed in Wangfu Street Quarry. We observed and described the lithology characteristics and fault structure characteristics of the three geological sections through field observation, field sampling, and photographing records. These collected rock samples were used for subsequent thin section production and permeability experiments.

We made a total of 19 thin sections from rock samples representing different parts of the fault damage zone and carried out the sedimentary structure observation, component identification, and microstructural observation. The thin sections were impregnated with blue-dyed resin and stained with Alizarin red to visualise porosity and differentiate between calcite and dolomite (Dickson 1966). We used a Nikon 50I-P100-L polarising microscope to observe the slices.

We used the seepage experimental system for low to ultra-low permeability rocks developed by the State

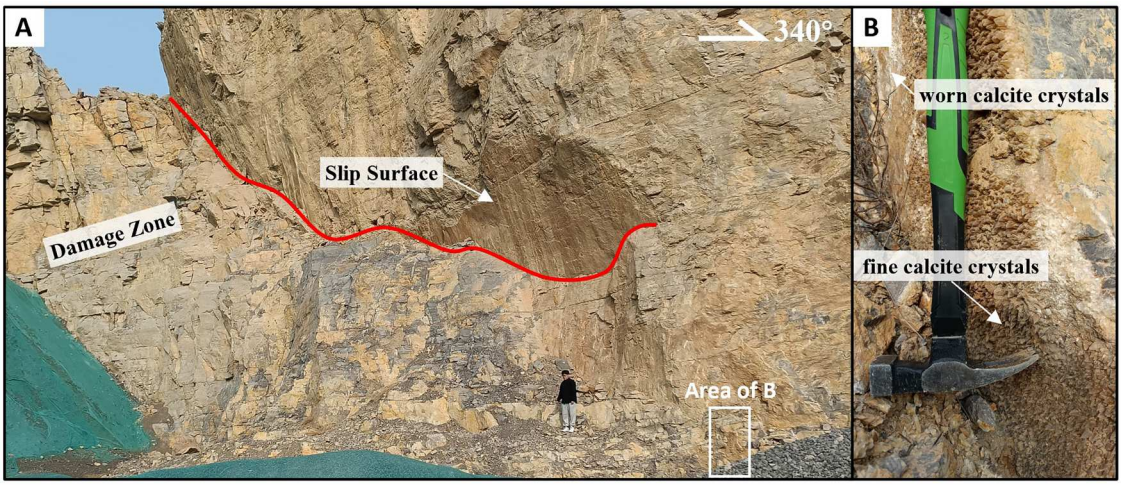

Figure 2. Outcrop photographs of WSF in the Wangfu Street quarry. The oucrop is Cambrian & Ordovician Sanshanzi Formation, striking 340°, GPS: 118°23′47.13″E, 36°40′3.59″N. (A) The red line delieanates the boundary between the slip surface and the damage zone. (B) Calcite crystals form at the slip surfaces, with both the worn crystals and the intact crystalline particles preserved.

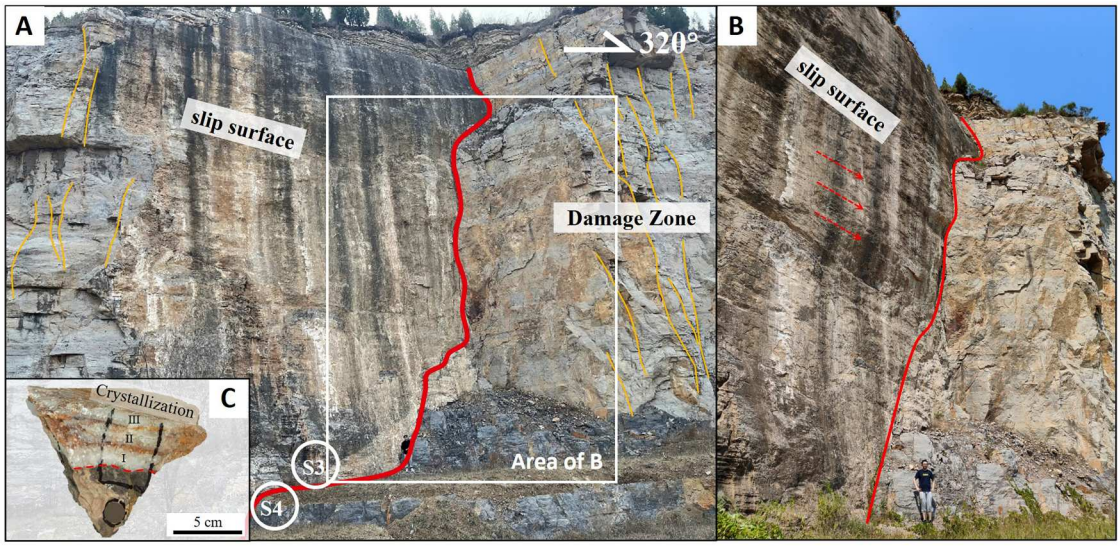

Figure 3. Outcrop photographs of TSF1 in the Tuoshan Nan quarry. The carbonate outcrop is Ordovician Majiagou Formation, striking 320°, GPS: 118°26′13.83″E, 36°37′57.51″N. (A) The fault line is represented by the red line, while the sub-faults and fractures are delineated by the yellow lines. The white circle marks the designated sampling positions for micro-flake fabrication and permeability experiments, respectively. (B) The direction of scratches on the slip surface is denoted by the red dotted arrow, confirming that TSF1 is characterised as a right-slip fault. (C) Photograph of sample S3, which is marked with multi-stage calcite cementation.

Key Laboratory of Seismic Dynamics, Institute of Geology, China Earthquake Administration to measure the permeability of the collected rock samples.

We used standard cylindrical samples with length of 5~20 mm and diameter of 19.5~20.5 mm and the liquid oscillation method for the permeability test.

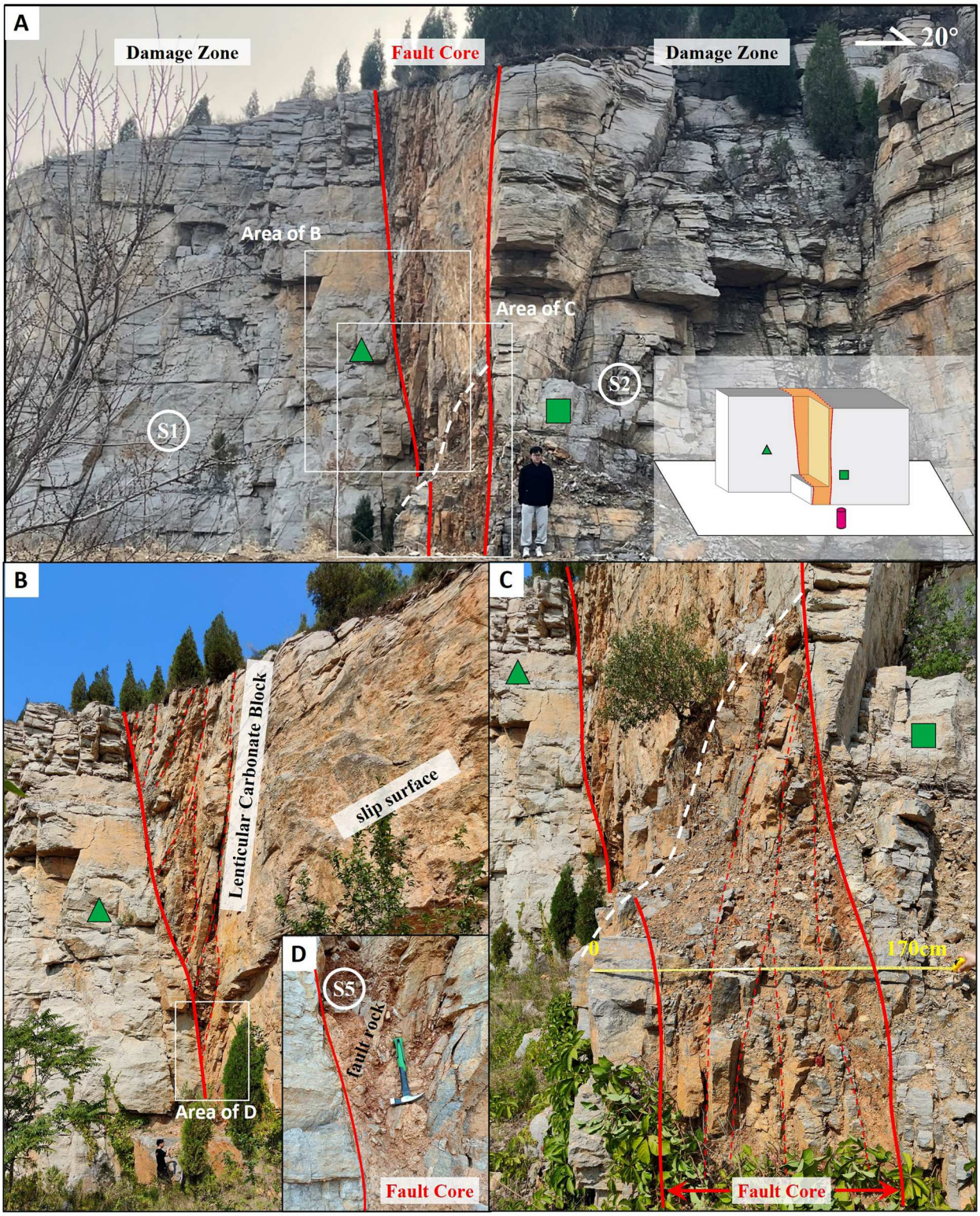

Figure 4. Outcrop photographs of TSF2 in the Tuoshan South quarry. The outcrop is Ordovician Majiagou Formation, striking 20°, GPS: 118°26′15.15″E, 36°37′54.61″N. (A) The red line indicates the location of the fault core boundary, and the white circle indicates the sampling position for micro-flake fabrication and permeability experiments, respectively. The lower part of the white dotted line is the cross-section of the fault core, and the upper part is the internal sliding surface and the distant cross-section of the fault core. The cartoon in the lower right corner reflects the three-dimensional view of the outcrop, in which the purple cylinder indicates the position of A, and the yellow shadow, green triangle, and green square correspond to A. (B) Remote view of the fault core. (C) 1 m wide fault core. Internal lenticular carbonate block and the red dotted line represents the boundary. (D) Fault rock and the sampling position.

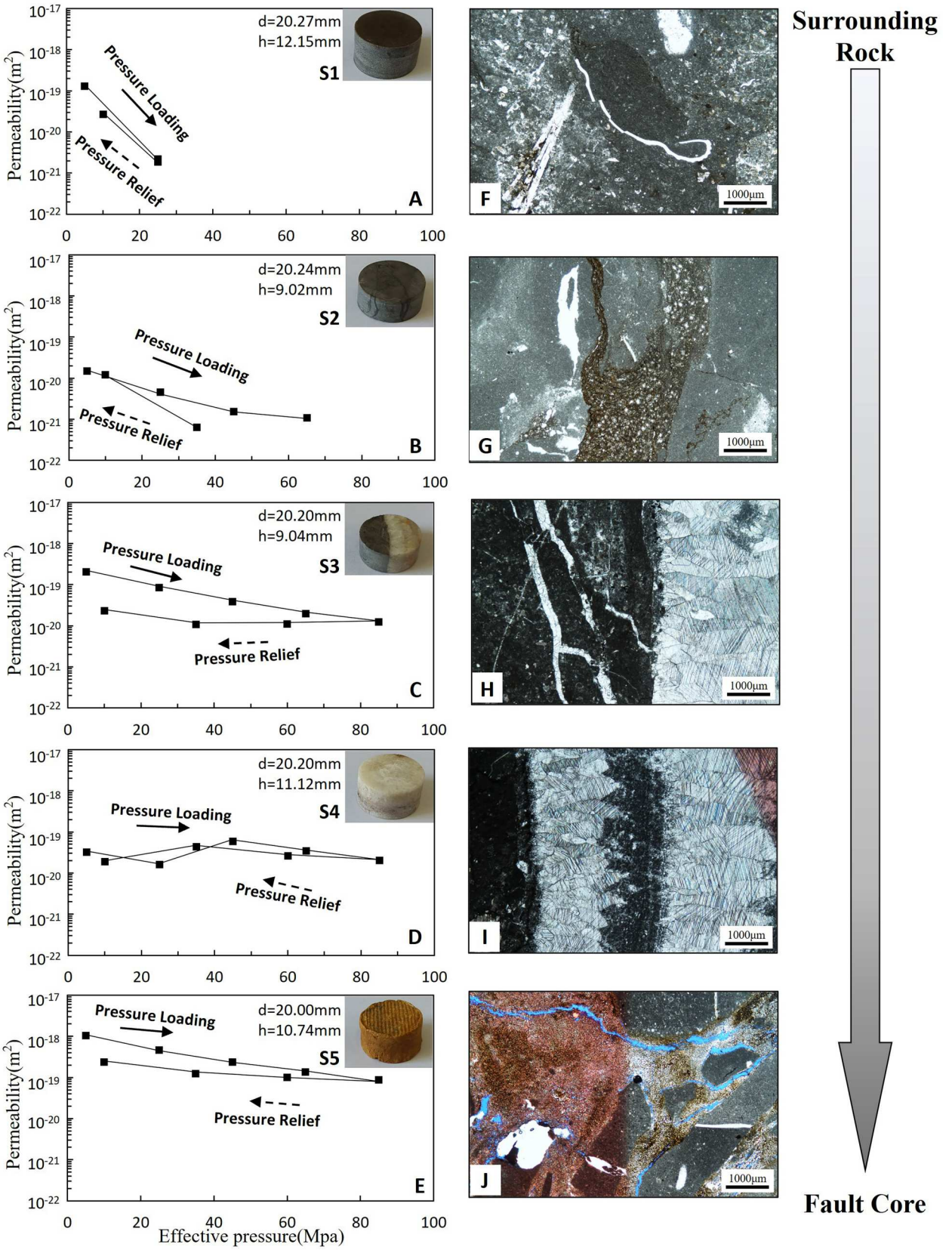

Figure 5. The permeability results obtained from field testing of rock samples and images captured under a microscope after thin-section preparation of the rock specimens. The location of the samples collected for permeability tests are marked as circular symbols of S1-S5 in TSF1 and TSF2 faults in Figures 3 and 4. Samples from S1 to S5 correspond, respectively, to the variations in the fault zone from surrounding rocks to the core of the fault. (A-E) The corresponding variations in permeability with increasing load pressure for samples, as well as the subsequent permeability results associated with unloading pressure. (F-J) Microscopic images corresponding to S1 to S5.

The oscillation method was originally proposed by Cowan (1961), drawing inspiration from techniques used to measure thermal diffusion coefficients. It was later refined and further developed by Kranz et al. (1990). This method has since been successfully applied in various experimental studies (e.g. Wu et al. 2011; Chen et al. 2013). In this approach, a controlled oscillatory pressure, typically sinusoidal, is applied to the upstream end of a core sample. The permeability of the sample induces a corresponding pressure response at the downstream end, which is characterised by a phase delay and a reduction in amplitude relative to the input signal. As an unsteady-state method, the pressure oscillation technique is particularly well-suited for measuring the permeability of low to ultra-low permeability rock samples. Its key advantages include high measurement accuracy, rapid data acquisition, and operational simplicity, making it an effective and reliable method for characterising fluid flow in tight geological formations.

Architecture of Fault Damage Zones

We analysed three typical faults in the Qingzhou area, including the Wangfu Street quarry Fault (WSF) and two faults in the Tuoshan Nan quarry (named TSF1 and TSF2). In general, they show the architecture of carbonate fault that contains: (1) Discrete, single, and planar slip surfaces or localised slip zones; and (2) Damage zones surrounding the slip surfaces.

Fault Damage Zones at Wangfu Street Quarry

The WSF fault is a 10-km scale strike-slip fault with damage zone at a thickness of more than 100–120 m featured by the presence of pervasive fractures (Figure 2). High density fractures are developed close to the fault surface and fracture density decreases towards the country rock away from the fault surface, similar to the observations in other studies (Palmer and Rice 1973; Engelder 1974; Aydin and Johnson 1978; Sibson 2003). These fractures extend metres long with no offset. Most of the fractures are shear, striking sub-parallel to the main slip surface (Figure 2(A)). There are no gouges in the slip surface but slip surfaces and fractures within the fault damage zone are mostly filled with a layer of calcite cement, 5–30 mm thick (Figure 2(B)), indicating the fracture network within the damage zones and the slip surface are connected hydraulically. In certain locations of slip surfaces, cm-scale calcite crystals are well developed, and some of which were worn with a second layer of crystalline particles deposited above (Figure 2(B)).

Fault Mirrors at Tuoshan Nan Quarry (TSF1)

All faults studied here contain slip surfaces, but the number of slip surfaces differ for different faults. Our field investigation indicates that faults without fault cores have one main slip surface (Figures 2 and 3), whereas faults with fault cores often have multiple slip surfaces (Figure 4).

TSF1 fault is a km class right-lateral strike-slip fault exposed in the Tuoshan Nan quarry, with a strike of 320° and an almost vertical fault. The outcrop is dolomite of Ordovician Majiagou Formation. The sliding surface between the two fault blocks is shown by the

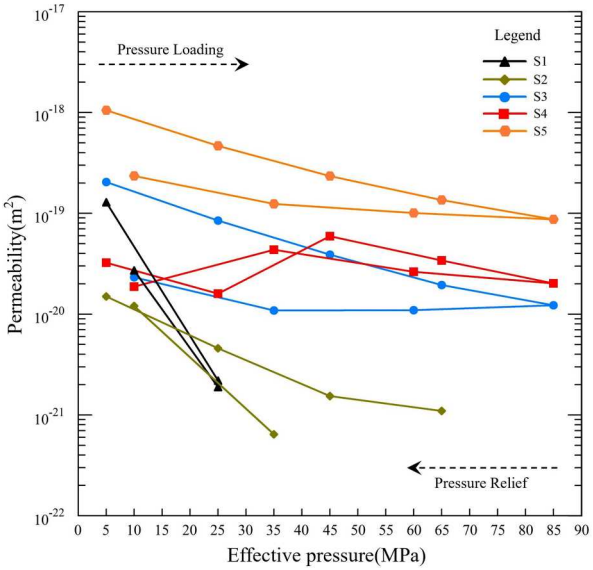

Figure 6. Experimental results of permeability of field samples. The results of the permeability of the sample during the loading and unloading confining pressure process.

Table 1. Experimental results of permeability of field samples

Sample Number	Tectonic Position	Lithology	Porosity (%)	Permeability ($\times10^{-20}$m^2)								
				Pressure Loading (MPa)					Pressure Relief (MPa)			
				5	25	45	65	85	60	35	25	10
S1	SR	Argillaceous Limestone	\	12.880	0.219	\	\	\	\	\	0.189	2.713
S2	DZ	Argillaceous Limestone	9.66	1.497	0.458	0.154	0.110	\	\	0.064	\	1.202
S3	DZ-FC	Argillaceous Limestone – Calcite	9.80	20.480	8.474	3.891	1.946	1.225	1.095	1.089	\	2.317
S4	FC (cement)	Calcite	9.68	3.238	1.599	5.938	3.413	2.019	2.632	4.360	\	1.871
S5	FC (fault gouge)	Clay	\	105.200	46.720	23.430	13.540	8.697	10.070	12.420	\	23.500

Note: SR represents surrounding rock, DZ represents damage zone, FC represents fault core. '\' represents no measurement result.

red line, and the associated sub-faults and cracks are shown by the yellow line (Figure 3). The exposed hundred-meter tall slip surface has a shiny crust representative for carbonate fault mirrors (Siman-Tov et al. 2015), and horizontal slip striations are visible even with strong weathering. Thin slices of the TSF1 sample show multistage crystallisation of calcite at the fracture surface (Figure 3(C), Figure 5(H), 2(I)). In each calcite cemented growth zone, the crystal morphology can be distinguished, and the grain boundaries are bounded by worn crystals (Central vertical black stripe in Figure 5(I)).

Fault Cores at Tuoshan Nan Quarry (TSF2)

The outcrop of TSF2 in Tuoshan Nan quarry is a strike-slip fault composed of Ordovician Majiagou formation of carbonate, striking 20°. The fault core consists of a 1-meterwide strip of distinct brown-yellow gouge, interspersed with multiple sub-parallel slip surfaces and lenticular cataclastic fragments ranging in size from 10 to 30 cm (Figure 4). Cataclastic rocks occurring in the fault core are commonly poorly indurated protocataclasites, cataclasites, and cataclasite fragments mainly consisting

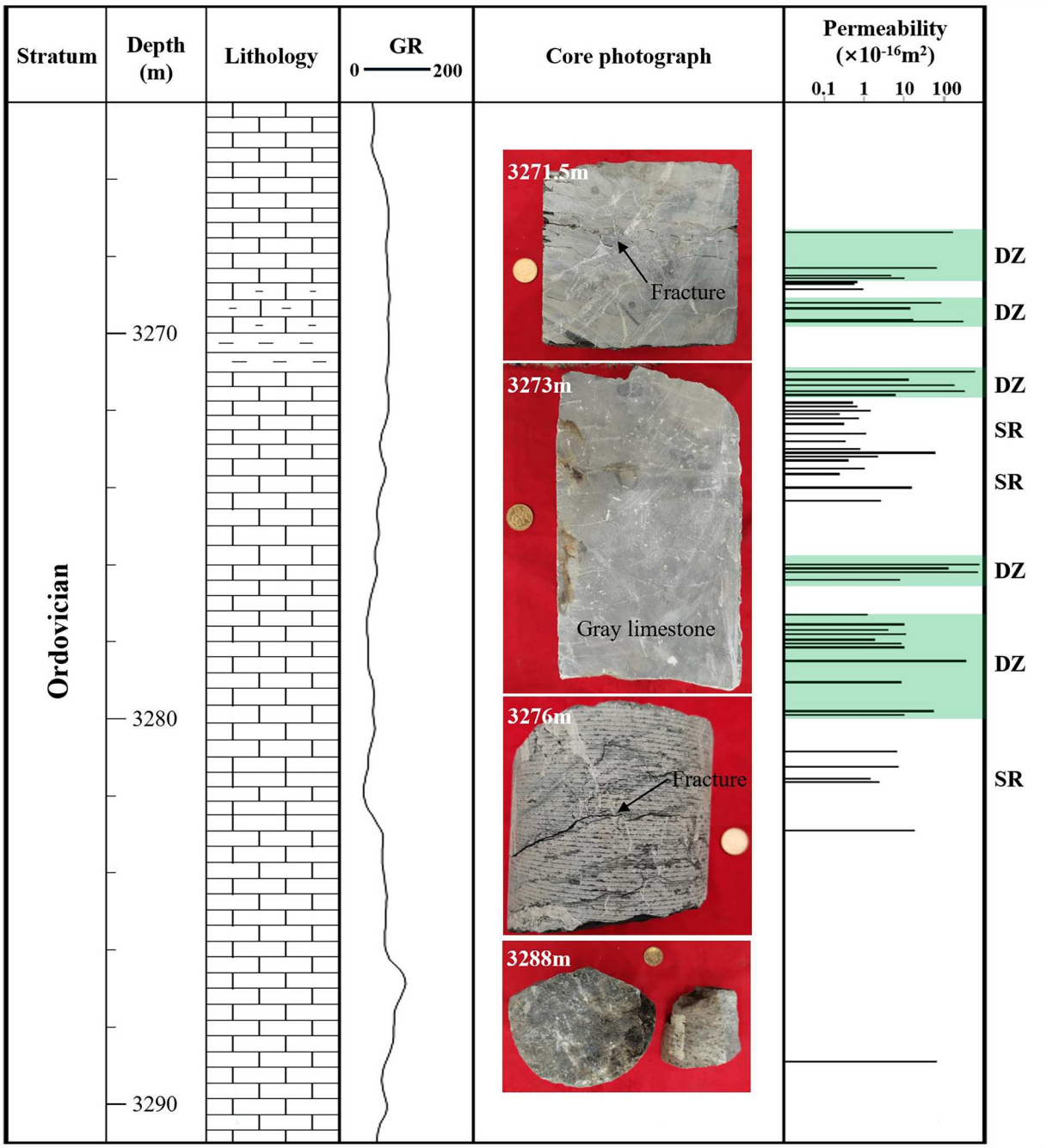

Figure 7. Well logging curves of some Ordovician formations drilled in X2, with depths ranging from 3264 to 3291.4 m. The core photos show that fractures developed in the fault damage zone (DZ) correspond to high permeability, and the surrounding rock (SR) corresponds to low permeability.

Table 2. Drilling core permeability data from Exploration and Development Research Institute, Shengli Oilfield Company, SINOPEC.

Well	Depth(m)	Equivalent effective pressure(MPa)	Stratum	Tectonic Position	Lithology	Density(g/cm^3)	Porosity (%)	Permeability ($\times10^{-16}$m^2)
X2	3267.37	54.43	O	DZ	Grey limestone	2.74	4.0	164.80
X2	3268.30	54.45	O	DZ	Grey limestone	2.68	4.6	65.80
X2	3268.50	54.45	O	SR	Grey limestone	2.68	5.6	4.90
X2	3268.57	54.45	O	SR	Grey limestone	2.63	7.2	9.93
X2	3268.67	54.46	O	SR	Grey limestone	2.62	7.4	0.68
X2	3268.72	54.46	O	SR	Grey limestone	2.65	6.9	0.57
X2	3268.85	54.46	O	SR	Grey limestone	2.65	6.5	0.96
X2	3269.20	54.46	O	SR	Grey limestone	2.63	7.0	82.14
X2	3269.35	54.47	O	SR	Grey limestone	2.59	8.9	14.91
X2	3269.65	54.47	O	SR	Grey limestone	2.46	12.6	16.26
X2	3269.70	54.47	O	DZ	Grey limestone	2.60	7.1	304.03
X2	3271.00	54.49	O	DZ	Grey limestone	2.63	2.9	596.24
X2	3271.20	54.50	O	DZ	Grey limestone	2.63	3.1	13.47
X2	3271.35	54.50	O	DZ	Grey limestone	2.63	2.9	180.01
X2	3271.50	54.50	O	DZ	Grey limestone	2.62	3.4	347.78
X2	3271.60	54.50	O	SR	Grey limestone	2.63	3.1	6.20
X2	3271.80	54.51	O	SR	Grey limestone	2.68	1.4	0.53
X2	3271.90	54.51	O	SR	Grey limestone	2.67	1.5	0.67
X2	3272.00	54.51	O	DZ	Grey limestone	2.68	1.3	1.40
X2	3272.10	54.51	O	SR	Grey limestone	2.68	1.3	0.25
X2	3272.20	54.51	O	SR	Grey limestone	2.67	1.4	0.77
X2	3272.35	54.52	O	SR	Grey limestone	2.67	1.5	0.33
X2	3272.60	54.52	O	SR	Grey limestone	2.67	1.7	1.14
X2	3272.80	54.52	O	SR	Grey limestone	2.67	1.4	0.35
X2	3273.00	54.53	O	SR	Grey limestone	2.67	1.5	0.83
X2	3273.10	54.53	O	DZ	Grey limestone	2.66	1.8	58.60
X2	3273.20	54.53	O	SR	Grey limestone	2.66	1.7	2.16
X2	3273.30	54.53	O	SR	Grey limestone	2.66	1.8	0.42
X2	3273.50	54.54	O	SR	Grey limestone	2.66	1.7	1.05
X2	3273.65	54.54	O	SR	Grey limestone	2.68	1.3	0.25
X2	3274.00	54.54	O	DZ	Grey limestone	2.65	2.2	15.87
X2	3274.35	54.55	O	SR	Grey limestone	2.65	2.1	2.63
X2	3276.00	54.58	O	DZ	Grey limestone	2.59	3.9	778.04
X2	3276.10	54.58	O	DZ	Grey limestone	2.62	3.4	132.00
X2	3276.20	54.58	O	DZ	Grey limestone	2.63	2.9	680.99
X2	3276.40	54.58	O	SR	Grey limestone	2.65	2.4	7.83
X2	3277.30	54.60	O	SR	Grey limestone	2.64	2.6	1.21
X2	3277.55	54.60	O	DZ	Grey limestone	2.64	2.7	10.37
X2	3277.70	54.61	O	SR	Grey limestone	2.65	2.3	4.05
X2	3277.80	54.61	O	DZ	Grey limestone	2.64	2.5	10.89
X2	3277.95	54.61	O	SR	Grey limestone	2.65	2.3	1.84
X2	3278.05	54.61	O	DZ	Grey limestone	2.65	2.0	8.50
X2	3278.15	54.61	O	DZ	Grey limestone	2.64	2.6	10.35
X2	3278.50	54.62	O	DZ	Grey limestone	2.64	2.4	364.11
X2	3279.05	54.63	O	DZ	Grey limestone	2.65	2.0	8.76
X2	3279.80	54.64	O	DZ	Grey limestone	2.61	3.5	54.70
X2	3279.90	54.64	O	DZ	Grey limestone	2.62	3.1	10.37
X2	3280.85	54.66	O	DZ	Grey limestone	2.63	2.8	6.76
X2	3281.25	54.67	O	DZ	Grey limestone	2.62	3.4	7.42
X2	3281.55	54.67	O	SR	Grey limestone	2.67	1.4	1.39
X2	3281.65	54.67	O	DZ	Grey limestone	2.67	1.3	2.38
X2	3282.90	54.69	O	DZ	Grey limestone	2.65	2.1	19.10
X2	3288.90	54.79	O	DZ	Grey limestone	2.82	1.5	62.42
X2	3291.20	54.83	O	DZ	Grey limestone	2.69	4.7	260.82

Note: SR represents surrounding rock, DZ represents damage zone. Pz represents Palaeozoic, O represents Ordovician. '\' represents no measurement result.

of single grains and fossil shells from calcarenites, grain and fossil fragment, and larger (up to a few centimetres) multigrain, angular calcarenite clasts (Figure 4(C)). They are surrounded by a finer calcareous cataclastic gouge matrix, which is significantly more abundant in the first few millimetres adjacent to the slip surfaces. Almost all the fault displacement is accommodated within the localised fault core, which represents a mature stage of fault development in the Qingzhou area (Micarelli et al. 2006).

Permeability Data

Field rock outcrops in the Qingzhou area were sampled across the fault zones. The location of the samples collected for permeability tests are marked as circular symbols of S1-S5 in TSF1 and TSF2 faults in Figures 3 and 4. For fault gouges, samples were taken directly from a steel pipe with an inner diameter of 20 mm. For cemented rocks, hand specimens were taken in the field and samples were drilled in the lab. Cylindrical samples of 10–20 mm in length were taken and a constant temperature of 80°C was set for more

than 72 h to dry the rock sample. The total porosity was measured by the gasometrical method (Table 1).

Table 1 presents the permeability measurements at different confining pressures (5–85 MPa). Figure 5 shows the change of permeability with the confining pressure, and some samples were tested under loading-unloading cycles.

A few permeability characteristics of the fault damage zones are observed: (1) the permeabilities of the fracture-filled damage zone are 1–2 orders of magnitude lower than that of the surrounding rock. (2) The permeability decreases rapidly as the effective pressure rises, and the rate of permeability decline of the surrounding rock is significantly faster than other rock samples. (3) The permeability response to pressure loading-unloading show that the difference in permeability between fault gouge and rocks is relatively small. The permeability of the fault gouge decreases rapidly with stress loading, while its recovery is lagged during unloading and rises slowly only after the effective pressure is less than 35 MPa.

Discussions

Permeability Structure of the Carbonate Fault

We plotted the above experimental test data in Figure 6. Figure 7 shows the drilling core photos and their permeability test data (Table 2).

The permeability profile in Figures 6 and 7 shows the variation of permeability in different components of a fault damage zone accordingly. The highest permeability (10^{-14} m^2) is found in the fault damage zone, followed by the surrounding rock with intermediate permeability ranging from 10^{-17} m^2 to 10^{-15} m^2, with the gouge filled fault core having the lowest permeability ($<10^{-18}$ m^2). The results suggest an increasing trend of permeability from protolith to damage zones and a decreasing trend of permeability from the damage zone to the fault core. Such a permeability profile across the fault suggests that: (1) sections of the fault core with well-consolidated gouge layer and strong cementation may serve as fluid barriers hindering fluid flow from entering the fault damage zone, as observed by previous studies (Antonellini and Aydin 1994, 1995; Caine et al. 1996); (2) the damage zone on two sides of the fault can be hyperpermeable in the direction parallel to the fault plane but possibly much less permeable in the direction perpendicular to the fault (Morrow et al. 1981; Tanikawa et al. 2009).

Implication for Damage Zone Evolution

The outcrops of TSF1 and TSF2 show that they are of similar scale and characteristics in damage zone. However, the differences in the fault core structure between the two are different, with TSF1 developing ~cm thick fault core with a major principal slip surface while TSF2 developing into a 1-m-thick fault core zone with multiple slip surfaces and gouges. Sush difference in fault core geometrical structures reflects different stages of fault evolutionary maturity in carbonate formations (Micarelli et al. 2006), which also determines the structure of fault permeability as documented in our study.

Based on our results, we propose the following major steps of fault development in the current case. At the early stage, only a few distributed fault surfaces may develop within the fault core, and these newly formed faults serve as preferred conduits for fluid flow at the fault core (Billi et al. 2003) (Figure 8(A)). The TSF1 is at the early stage, as supported by similar fault core structure with a few slip surfaces (Figure 3) and high permeability at fault core inferred from strong calcite mineral deposits on the slip surface (Figure 5(H)). With continued displacement, the fault core develops into a wide and discontinuous core zone to accommodate further deformation. The fault core zone consists of mainly fractured breccia and fractured rocks, and act as low permeability barriers for fluid flow (Figure 8(B)). In the mature stage with larger displacement, a continuous and wider fault core zone develops within the fault. This mature fault core zone contains fractured rocks, lenses, and fault gouges (TSF2, Figure 4 and 8(C)). Once a granular structure develops within the fault core zone (e.g. breccia), its further evolution is similar to the development of clastic deformation zones (Aydin and Johson, 1978, 1983; Antonellini and Aydin 1994), where rotation and abrasion of particles occur, leading to fragmentation of the adjacent rocks and enlargement the fault core. The thick layer of gouge and fluid-assisted mineral cementation within the fault core zone gives a complex and anisotropic pattern of permeability (Figure 8(C)), with the most permeable direction in sub-parallel to the fault slip surface.

During seismic cycles, rock properties within the damage zone, including permeability, changes over time (Chester and Logan 1986; Morrow and Byerlee 1992; Faulkner et al. 2010). These variations can affect stress and pore pressure distribution around the fault, friction and healing properties of the fault, and the sealing potential along the fault (Beeler and Lockner 2003; Faulkner et al. 2011). The current case study provides insights into how subsurface fluids migrate through carbonate faults and the interaction between fluid flow and fault sealing potential.

Conclusions

In this paper, we investigated carbonate faults in the Qingzhou area of eastern China using field

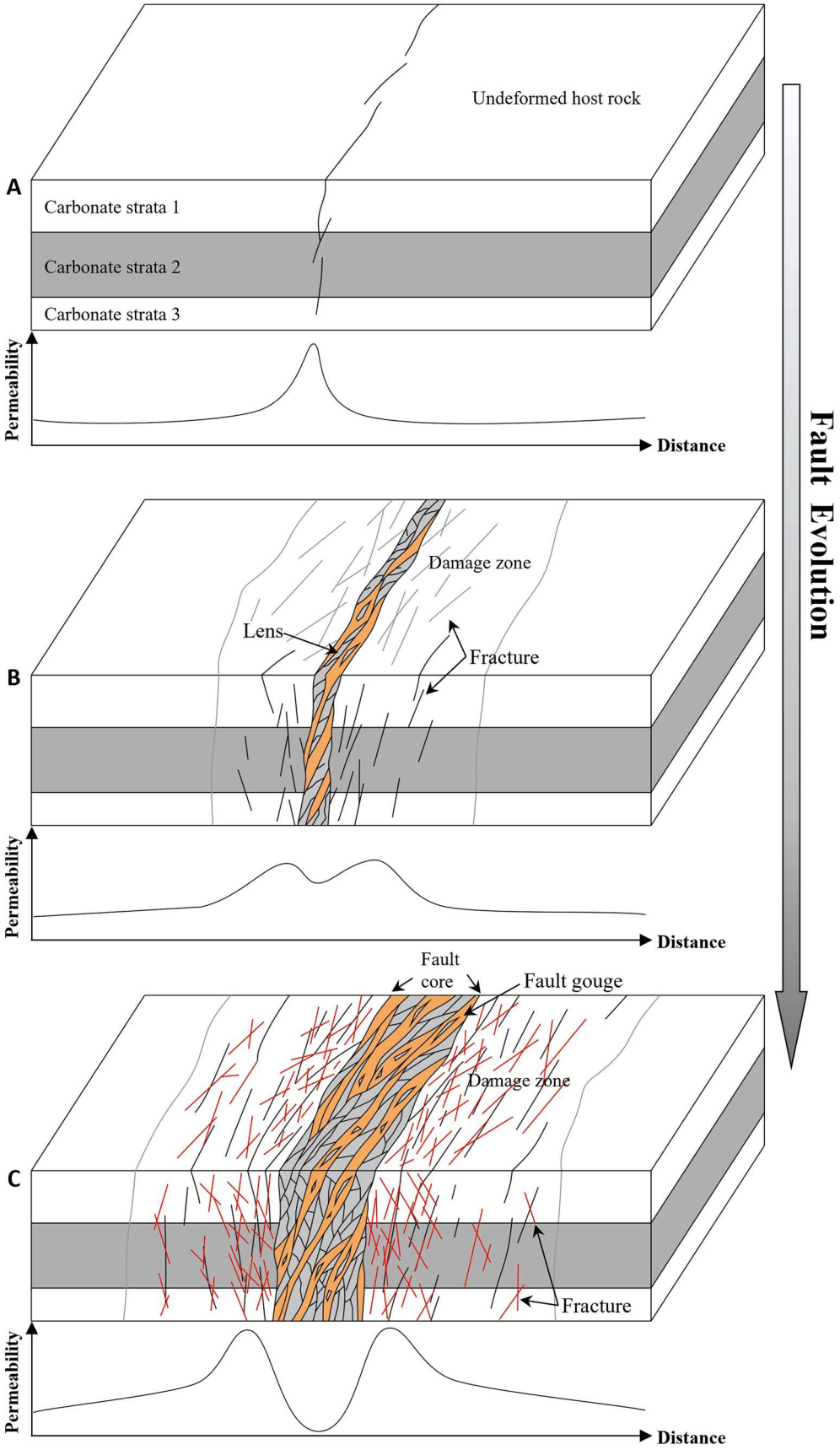

Figure 8. A three-dimensional model depicting the evolution of fault zones in carbonate rock formations, along with a schematic representation of the corresponding permeability within these fault zones. The solid grey line distinguishes the surrounding rock from the damage zone (A) Pre-existing or early-formed fractures typically develop perpendicular to the bedding orientation, and the corresponding fractured zones represent high-permeability areas. (B) As the fault zone evolves, the fractured areas continuously extend into the surrounding rock, gradually forming high-permeability damage zones along with narrow fault cores. (C) With the increasing evolution of the fault zone, it eventually forms a wide, ultra-low permeability fault core, and the permeability structure exhibits an 'm' shape.

investigation, rock sample analysis, thin section identification, and permeability test. We identified several different fault evolution patterns, e.g. drastic fault deformation of WSF and 'Fault mirror' of TSF1 are in the stage of early development with strong fluid flow inside the fault core, and the thick-fault core of TSF2 is in a mature stage with the fault core as fluid flow barriers. We conducted permeability experiments and summarised a permeability structure for the mature fault: fluid activity within the fault zone is confined to the high-permeable damage zones, and the fault core has low or ultra-low permeability. Therefore, fluids are prone to migrate parallel to the faults but difficult to flow perpendicular to the faults. Our case study documented how faults evolve within carbonate formations and how fluid flow varies in space and time within the fault zone, which has important implications for fluid transport through faulted rock bodies at the subsurface. We anticipate that the carbonate fault structures, their maturation level, and their permeability patterns may provide insights into the fault activities and seismic hazards.

Acknowledgments

The authors would like to thank the reviewers for their thoughtful and detailed reviews of the manuscript. We also like to thank Jianye Chen, Qingbao Duan, and Fuqi Cheng from the Institute of Geology, China Earthquake Administration, for their help in the experiments. We acknowledge Sinopec for providing drilling cores and samples. This work was supported by the National Key R&D Program of China 2024YFE0114000 (to ZL).

Disclosure statement

No potential conflict of interest was reported by the author(s).

Funding

This work was supported by the National Key R&D Program of China 2024YFE0114000 (to ZL).

Data availability statement

The data that support the findings of this study are available from the corresponding author, Zong, upon reasonable request.

ORCID

Nianfa Yang http://orcid.org/0009-0000-6148-2603

References

Antonellini M, Aydin A. 1994. Effect of faulting on fluid flow in porous sandstones: petrophysical properties. AAPG Bulletin. 78(3):355–377.

Antonellini M, Aydin A. 1995. Effect of faulting on fluid flow in porous sandstones: geometry and spatial distribution. AAPG Bulletin. 79(5):642–671.

Aydin A, Johnson AM. 1978. Development of faults as zones of deformation bands and as slip surfaces in sandstone. Pure and Applied Geophysics. 116:931–942.

Aydin A, Johnson AM. 1983. Analysis of faulting in porous sandstones. Journal of Structural Geology. 5(1):19–31.

Beeler NM, Lockner DA. 2003. Why earthquakes correlate weakly with the solid earth tides: effects of periodic stress on the rate and probability of earthquake occurrence. Journal of Geophysical Research: Solid Earth. 108(B8). doi:10.1029/2001JB001518.

Bense VF, Gleeson T, Loveless SE, Bour O, Scibek J. 2013. Fault zone hydrogeology. Earth-Science Reviews. 127:171–192.

Bense VF, Person MA. 2006. Faults as conduit-barrier systems to fluid flow in siliciclastic sedimentary aquifers. Water Resources Research. 42(5). doi:10.1029/2005WR004480.

Billi A, Salvini F, Storti F. 2003. The damage zone-fault core transition in carbonate rocks: implications for fault growth, structure and permeability. Journal of Structural Geology. 25(11):1779–1794.

Caine JS, Evans JP, Forster CB. 1996. Fault zone architecture and permeability structure. Geology. 24(11):1025–1028.

Chen J, Yang X, Yao L, Ma S, Shimamoto T. 2013. Frictional and transport properties of the 2008 wenchuan earthquake fault zone: implications for coseismic slip-weakening mechanisms. Tectonophysics. 603:237–256.

Chester FM, Evans JP, Biegel RL. 1993. Internal structure and weakening mechanisms of the San andreas fault. Journal of Geophysical Research: Solid Earth. 98(B1):771–786.

Chester FM, Logan JM. 1986. Implications for mechanical properties of brittle faults from observations of the punchbowl fault zone, California. Pure and Applied Geophysics. 124:79–106.

Cowan RD. 1961. Proposed method of measuring thermal diffusivity at high temperatures. Journal of Applied Physics. 32(7):1363–1370.

Davis GH, Reynolds SJ, Cruden AR. 1996. Structural geology of rocks and regions. Economic Geology and the Bulletin of the Society of Economic Geologists. 91(6):1163.

Dickson JAD. 1966. Carbonate identification and genesis as revealed by staining. Journal of Sedimentary Research. 36(2):491–505.

Engelder JT. 1974. Cataclasis and the generation of fault gouge. Geological Society of America Bulletin. 85(10):1515–1522.

Evans JP. 1990. Textures, deformation mechanisms, and the role of fluids in the cataclastic deformation of granitic rocks. Geological Society, London, Special Publications. 54(1):29–39.

Evans JP, Forster CB, Goddard JV. 1997. Permeabilities of fault-related rocks and implications for fault-zone hydraulic structure. Journal of Structural Geology. 19:1393–1404.

Faulkner DR, Jackson CA, Lunn RJ, Schlische RW, Shipton ZK, Wibberley C, Withjack MO. 2010. A review of recent developments concerning the structure, mechanics and fluid flow properties of fault zones. Journal of Structural Geology. 32:1557–1575.

Faulkner DR, Mitchell TM, Behnsen J, Hirose T, Shimamoto T. 2011. Stuck in the mud? earthquake nucleation and propagation through accretionary

forearcs. Geophysical Research Letters. 38(18). doi:10.1029/2011GL048552.
Gale JF, Reed RM, Holder J. 2007. Natural fractures in the barnett shale and their importance for hydraulic fracture treatments. AAPG Bulletin. 91(4):603–622.
He S, Chen J, Shu Y, Cui X, Shi K, Wei C, Shi Z. 2021. Efficient fault-tolerant information barrier coverage in internet of things. IEEE Transactions on Wireless Communications. 20(12):7963–7976.
Knipe RJ. 1997. Juxtaposition and seal diagrams to help analyze fault seals in hydrocarbon reservoirs. AAPG Bulletin. 81(2):187–195.
Kranz RL, Saltzman JS, Blacic JD. 1990. Hydraulic diffusivity measurements on laboratory rock samples using an oscillating pore pressure method. International Journal of Rock Mechanics and Mining Sciences. 27:345–352.
Liao Z, Liu H, Jiang Z, Marfurt KJ, Reches ZE. 2017. Fault damage zone at subsurface: A case study using 3D seismic attributes and a clay model analog for the Anadarko Basin, Oklahoma. Interpretation. 5(2):T143–T150.
LIU Mingwei. 1999. Genesis and evolution of shangwujing fault zone in central shandong province. Shandong Geology. 02:11–16.
Manzocchi T, Walsh JJ, Nell P, Yielding G. 1999. Fault transmissibility multipliers for flow simulation models. Petroleum Geoscience. 5(1):53–63.
Micarelli L, Benedicto A, Wibberley CAJ. 2006. Structural evolution and permeability of normal fault zones in highly porous carbonate rocks. Journal of Structural Geology. 28(7):1214–1227.
Morrow C, Shi LQ, Byerlee J. 1981. Permeability and strength of San andreas fault gouge under high pressure. Geophysical Research Letters. 8(4):325–328.
Morrow CA, Byerlee JD. 1992. Permeability of core samples from cajon pass scientific drill hole: results from 2100 to 3500 m depth. Journal of Geophysical Research: Solid Earth. 97(B4):5145–5151.
Nur A, Booker JR. 1972. Aftershocks caused by pore fluid flow? Science. 175(4024):885–887.
Olson JE. 2003. Sublinear scaling of fracture aperture versus length: an exception or the rule. Journal of Geophysical Research: Solid Earth. 108(B9). doi:10.1029/2001JB000419.
Palmer AC, Rice JR. 1973. The growth of slip surfaces in the progressive failure of over-consolidated clay. Proceedings of the Royal Society of London. A. Mathematical and Physical Sciences. 332(1591):527–548.
Shandong Provincial Bureau of Geology & Mineral Resources. 1991. Regional geology of Shandong Province. Beijing: Geological Publishing House; p. 6-10 (in Chinese).
Shepherd, M. 2009. Oil field production geology: AAPG Memoir 91 (91). Tulsa, Oklahoma: AAPG.
Shipton ZK, Evans JP, Kirchner D, Kolesar PT, Williams AP, Heath JE. 2004. Analysis of CO2 leakage through 'low-permeability' faults from natural reservoirs in the Colorado plateau, east-central Utah. Geological Society, London, Special Publications. 233:43–58.
Sibson RH. 2003. Thickness of the seismic slip zone. Bulletin of the Seismological Society of America. 93(3):1169–1178.
Siman-Tov S, Aharonov E, Boneh Y, Reches ZE. 2015. Fault mirrors along carbonate faults: formation and destruction during shear experiments. Earth and Planetary Science Letters. 430:367–376.
Tanikawa W, Sakaguchi M, Hirono T, Lin W, Soh W, Song SR. 2009. Transport properties and dynamic processes in a fault zone from samples recovered from TCDP Hole B of the Taiwan Chelungpu Fault Drilling Project. Geochemistry, Geophysics, Geosystems. 10(4). doi:10.1029/2008GC002269.
Wang H. 1995. Earthquake research and seismic zoning in Qingzhou, Shandong. Beijing: Seismological Press; p. 80–100 (in Chinese).
Wang H. 2011. Study on the division and correlation method of Mesozoic strata in Gudao exploration area of Shengli Oilfield [M.S. thesis]. Guilin: Guilin University of Technology (in Chinese).
Wibberley CA, Shimamoto T. 2003. Internal structure and permeability of major strike-slip fault zones: the median tectonic line in Mie Prefecture, Southwest Japan. Journal of Structural Geology. 25(1):59–78.
Wu M, Yang X, Chen J. 2011. The calibration of ultralow permeability measurement apparatus and preliminary experimental results. Seismology and Geology. 33(2):719–731 (in Chinese).
Yielding G, Øverland JA, Byberg G. 1999. Characterization of fault zones for reservoir modeling: An example from the gullfaks field, northern north Sea. AAPG Bulletin. 83(6):925–951.
Yu D. 1992. The structure environment, rock-magma system, mineral -forming series and pattern of volcanic mineral-forming of uranium deposit in southeast of China. Journal of East China University of Technology(Natural Science). 01:11–22 (in Chinese).